Detecting insulitis in type 1 diabetes with ultrasound phase-change contrast agents

David G. Ramirez[a], Mark Ciccaglione[a], Awaneesh K. Upadhyay[b], Vinh T. Pham[a], Mark A. Borden[b,c], and Richard K. P. Benninger[a,d,1]

[a]Department of Bioengineering, University of Colorado Anschutz Medical Campus, Aurora, CO 80045; [b]Department of Mechanical Engineering, University of Colorado, Boulder, CO 80309; [c]Biomedical Engineering Program, University of Colorado, Boulder, CO 80309; and [d]Barbara Davis Center for Diabetes, University of Colorado Anschutz Medical Campus, Aurora, CO 80045

Edited by Matthias Von Herrath, La Jolla Institute for Immunology, La Jolla, CA, and accepted by Editorial Board Member Philippa Marrack August 13, 2021 (received for review October 28, 2020)

Type 1 diabetes (T1D) results from immune infiltration and destruction of insulin-producing β cells within the pancreatic islets of Langerhans (insulitis). Early diagnosis during presymptomatic T1D would allow for therapeutic intervention prior to substantial β-cell loss at onset. There are limited methods to track the progression of insulitis and β-cell mass decline. During insulitis, the islet microvasculature increases permeability, such that submicron-sized particles can extravasate and accumulate within the islet microenvironment. Ultrasound is a widely deployable and cost-effective clinical imaging modality. However, conventional microbubble contrast agents are restricted to the vasculature. Submicron nanodroplet (ND) phase-change agents can be vaporized into micron-sized bubbles, serving as a microbubble precursor. We tested whether NDs extravasate into the immune-infiltrated islet microenvironment. We performed ultrasound contrast-imaging following ND infusion in nonobese diabetic (NOD) mice and NOD;Rag1ko controls and tracked diabetes development. We measured the biodistribution of fluorescently labeled NDs, with histological analysis of insulitis. Ultrasound contrast signal was elevated in the pancreas of 10-wk-old NOD mice following ND infusion and vaporization but was absent in both the noninfiltrated kidney of NOD mice and the pancreas of Rag1ko controls. High-contrast elevation also correlated with rapid diabetes onset. Elevated contrast was also observed as early as 4 wk, prior to mouse insulin autoantibody detection. In the pancreata of NOD mice, infiltrated islets and nearby exocrine tissue were selectively labeled with fluorescent NDs. Thus, contrast ultrasound imaging with ND phase-change agents can detect insulitis prior to diabetes onset. This will be important for monitoring disease progression, to guide and assess preventative therapeutic interventions for T1D.

type 1 diabetes | autoimmunity | ultrasound | phase-change contrast agent | nanodroplets

Type 1 diabetes (T1D) is caused by infiltration of autoreactive immune cells into the islets of Langerhans in the pancreas (insulitis) and destruction of insulin-secreting β-cells. The subsequent loss of glucose homeostasis requires lifelong insulin therapy, with T1D subjects still at an elevated risk of chronic diabetes complications and hypoglycemia-induced coma or death. Prior to clinical onset, there exists an asymptomatic phase of many years where autoimmunity and insulitis progresses but glucose homeostasis is maintained (presymptomatic T1D) (1). However, patients with T1D are not diagnosed until presentation of hyperglycemia, where the majority of β-cell mass (>80%) has been lost. As such, this presymptomatic phase of T1D provides an ideal window for therapeutic prevention (2).

There has been some limited success in trials applying immunomodulatory agents designed to preserve β-cell mass and reverse or prevent T1D (3). For example, antiCD3 has recently been applied in first-degree relatives at high risk for T1D and showed a significant delay and reduced incidence of T1D onset (4). However, prevention was not complete, and these subjects were still significantly advanced in T1D progression, showing signatures of dysglycemia. Application of therapies at T1D onset similarly show only a temporary preservation of β-cell mass (as measured by c-peptide release), with a broad heterogeneity in treatment response (4). As such, earlier therapeutic treatment is desirable.

There are currently very limited means to determine whether a subject shows presymptomatic T1D. Furthermore, there are no means to assess the success or failure of therapeutic interventions beyond the onset of T1D itself. The presence of multiple islet-associated autoantibodies in circulation can determine risk of developing T1D within a multiyear time frame (5, 6). However, islet-associated autoantibodies are not pathogenic and cannot inform on successful therapeutic treatments. As such, there is a need to develop new methods to track the progression of insulitis and β-cell mass decline during presymptomatic T1D. Furthermore, at clinical onset there is a high incidence of diabetic ketoacidosis (DKA) that can have severe health consequences (7). Thus identifying "at-risk" subjects and monitoring their underlying disease progression will be important to mitigate the consequences of DKA.

Several imaging approaches have been explored to detect insulitis and β-cell mass decline (8–11). During insulitis, the islet

Significance

Methods to detect type 1 diabetes (T1D) progression prior to clinical diagnosis are needed. T1D results from autoreactive T cells infiltrating the islets of Langerhans, destroying insulin-producing β-cells. Overt disease takes years to present, and at diagnosis, there is substantial β-cell loss. Therapeutic intervention to preserve β-cell mass is hampered by an inability to follow presymptomatic T1D progression. Several immunotherapies can delay T1D development. However, identifying "at-risk" individuals and tracking whether therapeutic interventions are impacting disease progression, are lacking. We present ultrasound imaging of nanodroplet (ND) contrast-agent accumulation within the islet. ND accumulation is dependent on immune infiltration; therefore, it tracks presymptomatic T1D development and progression to diabetes. This provides an opportunity to guide therapeutic treatments to prevent T1D.

Author contributions: M.A.B. and R.K.P.B. designed research; D.G.R., M.C., A.K.U., V.T.P., and R.K.P.B. performed research; D.G.R. and M.C. analyzed data; and D.G.R. and R.K.P.B. wrote the paper.

The authors declare no competing interest.

This article is a PNAS Direct Submission. M.V.H. is a guest editor invited by the Editorial Board.

[1]To whom correspondence may be addressed. Email: richard.benninger@cuanschutz.edu.

This article contains supporting information online at https://www.pnas.org/lookup/suppl/doi:10.1073/pnas.2022523118/-/DCSupplemental.

Published October 4, 2021.

microvasculature increases permeability (11, 12). The enhanced permeability and retention (EPR) effect can therefore be used, where submicron-sized agents can accumulate in the inflamed islet microenvironment. This effect has been demonstrated using MRI contrast agents, in both mouse models of T1D and human T1D (13, 14). While promising, MRI modalities carry some limitations in terms of deployability and cost-effectiveness. Ultrasound imaging modalities can be widely deployed, are cost-effective, and provide real-time imaging. Contrast-enhanced ultrasound uses gas filled microbubbles and nonlinear signal detection. However, conventional microbubble contrast agents are restricted to the vasculature. Submicron-sized nanobubble ultrasound contrast agents have been developed that accumulate in tumors and inflamed tissue, including the immune infiltrated pancreas (15, 16). However, one potential limitation with submicron-sized bubbles is their low scattering cross-section, requiring a larger number of bubbles to be infused to generate measurable signal.

Nanodroplet phase-change agents are a class of submicron-sized ultrasound contrast agents (17, 18). Nanodroplets consist of a superheated gas core and folded lipid shell that are stable at body temperature. However, within an acoustic beam these nanodroplets (NDs) can vaporize into micron-sized bubbles that provide significant ultrasound contrast. As such, these NDs can act as a circulating nanoscale microbubble "precursor" to be "activated" by an acoustic beam. Nanodroplets can be readily formed by condensing conventional microbubble agents (19), including clinically approved agents (20). Given their submicron size, NDs have been demonstrated to follow the EPR effect and accumulate in tumors and generate measurable ultrasound contrast signals (19, 21). However, whether NDs can similarly accumulate in inflamed tissues and whether this accumulation can be measured and used for disease monitoring has been lacking.

In this study, we tested whether ND phase-change contrast agents specifically accumulate within inflamed islets of Langerhans in mouse models of T1D and the degree to which this accumulation depends on the level of insulitis. We further tested whether this accumulation could be measured noninvasively via ultrasound contrast imaging, as an increase in contrast signal following ND vaporization, and how this correlated with diabetes onset.

Results

Submicron NDs Accumulate and Can Be Vaporized within the Pancreas of Nonobese Diabetic Mice. Submicron-sized particles selectively accumulate in the islets of Langerhans in mouse models of T1D via the EPR effect that can occur in inflamed tissues (12, 15). Nanodroplet phase-change agents are submicron-sized particles that can accumulate in tumors and can be vaporized within the tissue to provide significant ultrasound contrast. We first tested whether NDs would similarly accumulate within immune-infiltrated islets of Langerhans and provide significant ultrasound contrast following vaporization. Size-isolated microbubbles were prepared and condensed under high pressure and low temperature into submicron-sized droplets (Fig. 1*A*). We utilized 10-wk-old female nonobese diabetic (NOD) mice where the immune-infiltrated pancreas and nonimmune-infiltrated kidney can be readily identified under conventional B-mode ultrasound imaging, with the spleen and kidney serving as a landmark for pancreas identification (Fig. 1*B*).

To measure whether NDs accumulate within the islet of NOD mice, we designed a protocol to separate NDs in circulation from tissue accumulation (Fig. 1*C*). First, a region was defined that covered either the pancreas (and spleen) or the kidney (Fig. 1*B*). Next, a series of subharmonic contrast mode images were acquired for 3 min prior to ND infusion, forming the background time courses. Following ND infusion, acquisition of conventional B-mode and contrast-mode images was paused for 25 min to allow maximal accumulation within inflamed tissues. This pause is based upon both size-isolated microbubbles and nanobubble contrast agents clearing from circulation within 5 to 15 min (11). Following this pause, a series of subharmonic contrast mode images were acquired for 10 min while the defined region was insonified and NDs vaporized (Fig. 1*C*). For both the pancreas/spleen region (Fig. 1*D*) and the kidney region (Fig. 1*E*), we compared the contrast signal prior to infusion with the contrast signal in each region during ND vaporization. Following ND infusion, increased contrast signal over the background was observed in the pancreas within ~3 min of insonifying the pancreas region (Fig. 1 *D* and *F*). After this time there was no further significant elevation in contrast signal. Within the kidney we observed no such elevation in contrast signal while insonifying the kidney region (Fig. 1 *E* and *F*). The increase in contrast signal within the pancreas 5 min after insonification was significantly elevated compared with the contrast signal within the kidney or spleen (Fig. 1*G*). These results suggest that NDs are specifically accumulating within the pancreas where immune-infiltrated islets of Langerhans are located, and these NDs can be vaporized within the tissue to provide measurable ultrasound contrast.

Submicron ND Accumulation Is Specific to Animals that Develop Diabetes. Given the lack of contrast elevation in the kidney of NOD mice, we next asked whether ND accumulation was specifically associated with immune cell infiltration. We compared 10-wk-old female NOD mice to age-matched and sex-matched immune deficient NOD;Rag1ko (Rag1ko) mice. In each case, we followed the same imaging protocol as before, focused on the pancreas (Fig. 2 *A* and *B*). Rag1ko mice do not develop mature T and B cells and thus do not show any immune cell infiltration into the islet and do not develop diabetes. As above, in NOD mice we observed a substantial elevation in contrast signal within ~3 min of insonification, indicating vaporization of accumulated NDs in the pancreas (Fig. 2 *A* and *C*). However, in the pancreas of NOD Rag1ko mice, we did not observe any contrast elevation following insonification of the pancreas (Fig. 2 *B* and *C*), indicating a lack of any ND accumulation and vaporization. The increase in contrast signal within the pancreas 5 min after insonification was significantly elevated in NOD mice compared with Rag1ko mice (Fig. 2*D*). Similar results were obtained if we used a more restricted pancreas region (*SI Appendix*, Fig. S1).

Submicron ND Accumulation Correlates with Diabetes Development. While NOD mice show significant insulitis at 10 wk of age (22), they do not become hyperglycemic until after 12 wk of age and show a wide range of ages at which diabetes develops (12 to 40 wk of age). Glucose measurements of female NOD mice were consistent with these reported numbers, where mice developed diabetes between 12 and 39 wk of age (Fig. 3*A*). Prior to 12 wk of age, ad libitum glucose levels were unchanged (Fig. 1*B*). Interestingly, we observed a significant correlation between the mean elevated contrast signal in the pancreas upon ND vaporization with the time from the measurement at which diabetes arises (Fig. 3*C*). Thus, mice that show elevated ultrasound contrast, associated with increased ND accumulation within the pancreas, progress more rapidly to diabetes. To test whether ND accumulation and elevated ultrasound contrast is observed at earlier time points, we followed the same imaging protocol as before, focused on the pancreas, in NOD mice at 4, 7, and 10 wk of age (Fig. 3*A*). The increase in contrast signal within the pancreas was significantly lower at 4 and 7 wk compared with at 10 wk (Fig. 3*D*). However, the contrast was still above baseline in the majority of animals at each time point. For those NOD mice that remained diabetes-free at 15 wk of age, the increase in contrast signal within the pancreas was less than that measured at 10 wk (*SI Appendix*, Fig. S2).

We then compared these ND accumulation measurements with established autoantibody measurement. Mouse insulin autoantibody

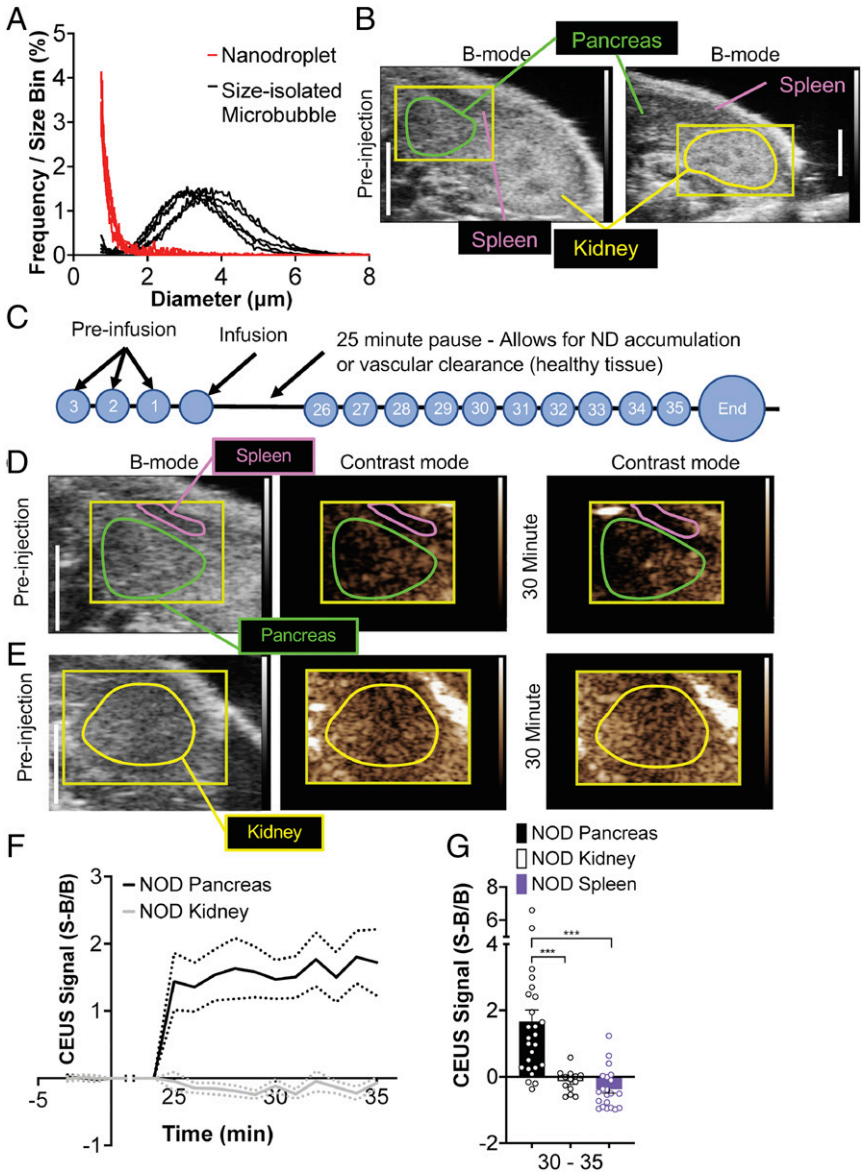

Fig. 1. ND infusion and vaporization increases contrast in the pancreas prior to T1D. (*A*) Size distribution of size-isolated microbubbles prior to condensation and of NDs following condensation. (*B*) Representative B-mode images of the abdomen, indicating the two regions in which vaporization was performed (pancreas, green; kidney, yellow), as well as the spleen anatomical landmarks used to identify the pancreas. (*C*) Schematic of ND imaging protocol, where time courses are recorded prior to ND infusion (preinfusion). After ND infusion, acquisition is paused to allow the NDs to accumulate in tissues with permeable microvasculature and clear from the bloodstream. Following the pause, time courses are then recorded for 10 min, during which droplets are vaporized. (*D*) Representative B-mode and subharmonic contrast images of pancreas (green) and spleen (purple) before ND infusion and 30 min after ND infusion. (*E*) As in *D* of the kidney. (*F*) Time-course of mean contrast signal, normalized to background, in the pancreas and kidney of 10-wk-old female NOD mice following ND infusion and vaporization. (*G*) Mean contrast signal averaged between 30 and 35 min following ND infusion for the pancreas, kidney, and spleen. Dashed lines in *F* represent 95% CI, error bars in *G* represent SEM. Data in *F* and *G* are representative of $n = 26$ mice (pancreas) and $n = 13$ mice (kidney). The *P* values in *G* are 0.0009 (***$P < 0.001$) comparing pancreas versus kidney and 0.0001 (***$P < 0.001$) comparing pancreas versus spleen (paired Student's *t* test). In *G*, an outlier data point (pancreas, S–B/B = 10.79) is not shown.

(mIAA) levels were measured at the same 4, 7, and 10 wk time points. We observed that the number of mIAA positive measurements increased over time (Fig. 3*E*), similar to the proportions observed in prior studies (23). However, at each time point the number of positive cases was lower than the number of cases in which elevated ultrasound contrast was above that measured in Rag1ko pancreas (i.e., exceeding 95% CI, Fig. 1*F*)

ND Accumulation within the Pancreas of NOD Mice Is Restricted to the Islet Environment. The pancreas contains two distinct compartments: the islets of Langerhans (endocrine pancreas) where immune cell infiltration occurs in NOD mice and the exocrine pancreas where immune cell infiltration is minimal. To determine the biodistribution of NDs within the pancreas undergoing insulitis, we infused DiO-labeled polydisperse NDs into 10-wk-old NOD mice and vaporized these NDs in a subset of mice following the same procedure as above (Fig. 1 and Fig. 2). Following ND vaporization (or a pause for those where NDs were not vaporized) we dissected and sectioned the pancreas for histological analysis. Following infusion and vaporization, NDs generated from (unlabeled) polydisperse microbubbles show elevated contrast signals in the pancreas but not in the kidney (*SI Appendix*, Fig. S3), similar to that measured in NDs generated from size-isolated microbubbles.

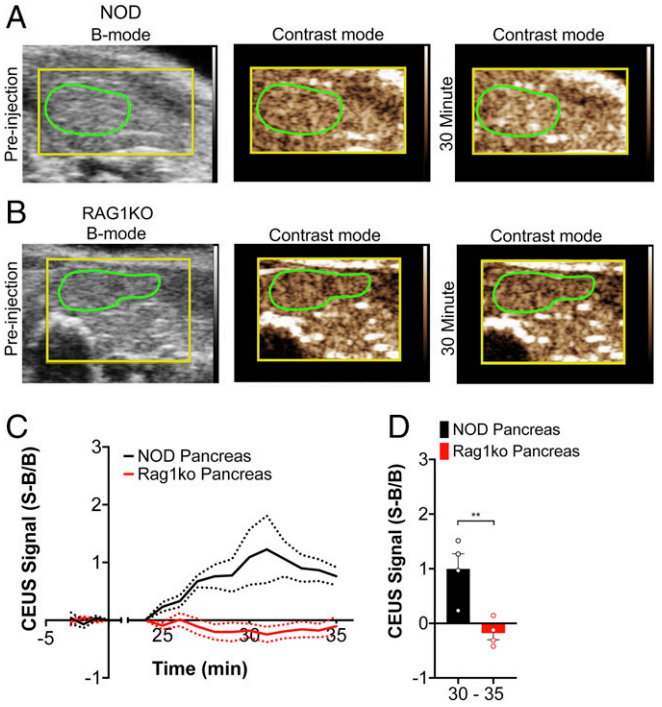

Fig. 2. ND infusion and vaporization increases contrast, dependent on insulitis and T1D. (*A*) Representative B-mode and subharmonic contrast images of the pancreas (green) before and 30 min. after ND infusion in 10-wk-old female NOD mice. (*B*) As in *A*, but for 10-wk-old immune-deficient female NOD;Rag1ko (Rag1ko) mice. (*C*) Time-course of mean contrast signal, normalized to background, in the pancreas of 10-wk-old female NOD mice versus 10-wk-old female Ragk1o mice following ND infusion and vaporization. (*D*) Mean contrast signal averaged between 30 and 35 min following ND infusion. Dashed lines in *C* represent 95% CI, and error bars in *D* represent SEM. Data in *C* and *D* are representative of $n = 4$ mice (NOD) and $n = 4$ mice (Rag1ko). The *P* value in *D* is 0.0083 (**$P < 0.01$) comparing groups indicated (unpaired Student's *t* test).

We first assessed the coverage of DiO fluorescence in the pancreas; within the islets, in regions close to the islet (within 200 μm, "near islet"); and within the exocrine pancreas far (>500 μm) from the islet (Fig. 4 *A*–*C*). We also compared the coverage of DiO fluorescence in these pancreas regions for vaporized and nonvaporized NDs (Fig. 4 *A* and *D*). In 10-wk-old NOD mice with vaporized NDs, the islet region showed significantly more fluorescent coverage compared with exocrine pancreas far from the islet (Fig. 4*E*). Fluorescence coverage in "near islet" regions showed an intermediate level (Fig. 4*E*). The fluorescence coverage within islet regions was marginally less ($P = 0.06$) in the pancreata of animals where there was no vaporization, compared with animals where NDs were vaporized (Fig. 4*F* and *SI Appendix*, Fig. S4). The fluorescence coverage within islet regions was also significantly greater in the pancreata of NOD mice compared with the pancreata of Rag1ko mice (Fig. 4*G*). Thus, NDs target the islet and near islet regions more favorably compared with exocrine regions in NOD mice but not in Rag1ko mice that lack insulitis.

To determine if ND accumulation is dependent on the level of insulitis, and thus underlying disease, we scored the level of insulitis in hematoxylin and eosin (H&E)-stained sections adjacent to those in which we measured DiO fluorescent coverage (Fig. 4*H*). Pancreata from Rag1ko islets showed no insulitis (Fig.4*I*). In pancreata from 10-wk-old NOD mice, the mean DiO coverage across islet regions of the pancreas was significantly correlated with the mean insulitis score across islets of the same pancreas (Fig. 4*J*, $P = 0.007$). Because we used adjacent sections when performing histology, we then examined insulitis on an islet-by-islet basis. Interestingly, there was no relationship between islet insulitis and fluorescent coverage (Fig. 4*K*): islets in which no insulitis was observed (score 0) showed similar DiO fluorescent coverage as islets in which substantial insulitis is observed (score 3). This is consistent with other reports in which the vascular permeability reflects the overall diseased state of the pancreas rather that the local level of disease (15). Consistent with measurements above, there was no relationship between fluorescent coverage and insulitis for nonvaporized NDs, whether analyzed by pancreas or by islet (*SI Appendix*, Fig. S4). Taken together, this demonstrates that within the NOD mouse NDs specifically

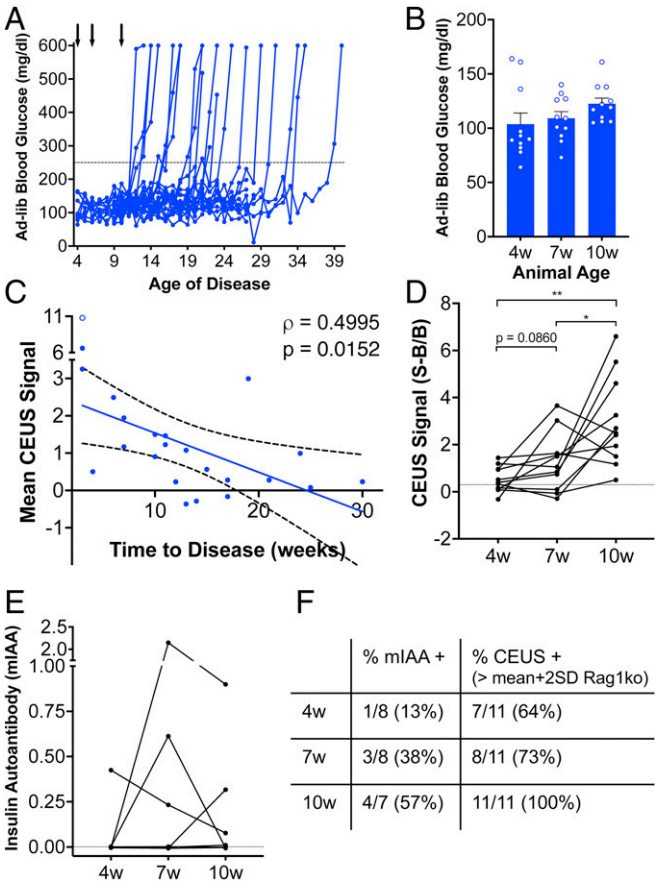

	% mIAA +	% CEUS + (> mean+2SD Rag1ko)
4w	1/8 (13%)	7/11 (64%)
7w	3/8 (38%)	8/11 (73%)
10w	4/7 (57%)	11/11 (100%)

Fig. 3. ND contrast elevation correlates with T1D onset in NOD mice. (*A*) Time course of ad libitum measured blood glucose in the NOD mice that received ND infusion. Arrows indicates time points of ND infusion and ultrasound scans. (*B*) Mean ad libitum blood glucose levels at 4, 7, and 10 wk of age prior to mice developing diabetes. (*C*) Scatterplot of mean contrast elevation against the time to diabetes onset for the pancreas of NOD mice measured at 10 wk of age. (*D*) Mean contrast elevation (averaged between 30 and 35 min following ND infusion) within the pancreas of NOD mice at 4, 7, and 10 wk of age prior to mice developing diabetes. Dashed line indicates the mean +2 SD of the contrast elevation measured in Rag1ko mice. (*E*) Index of mIAA levels measured in NOD mice at 4, 7, and 10 wk of age prior to mice developing diabetes. Dashed line indicates limit of detection. (*F*) Proportion of NOD mice that were mIAA positive or that showed a contrast elevation above baseline (as determined from Rag1ko mice) at each time point in *D* and *E*. Data in *B* and *D* represent $n = 11$ NOD mice, data in *C* represent $n = 23$ NOD mice (1 outlier, Grubbs test, empty circle), and data in *E* represent $n = 8$ NOD mice. A mixed-effects model was used to assess the statistical significance and generate the regression in *C*. The *P* value in *D* is 0.0013 (**$P < 0.01$) and 0.0376 (*$P < 0.05$), comparing conditions indicated (paired Student's *t* test).

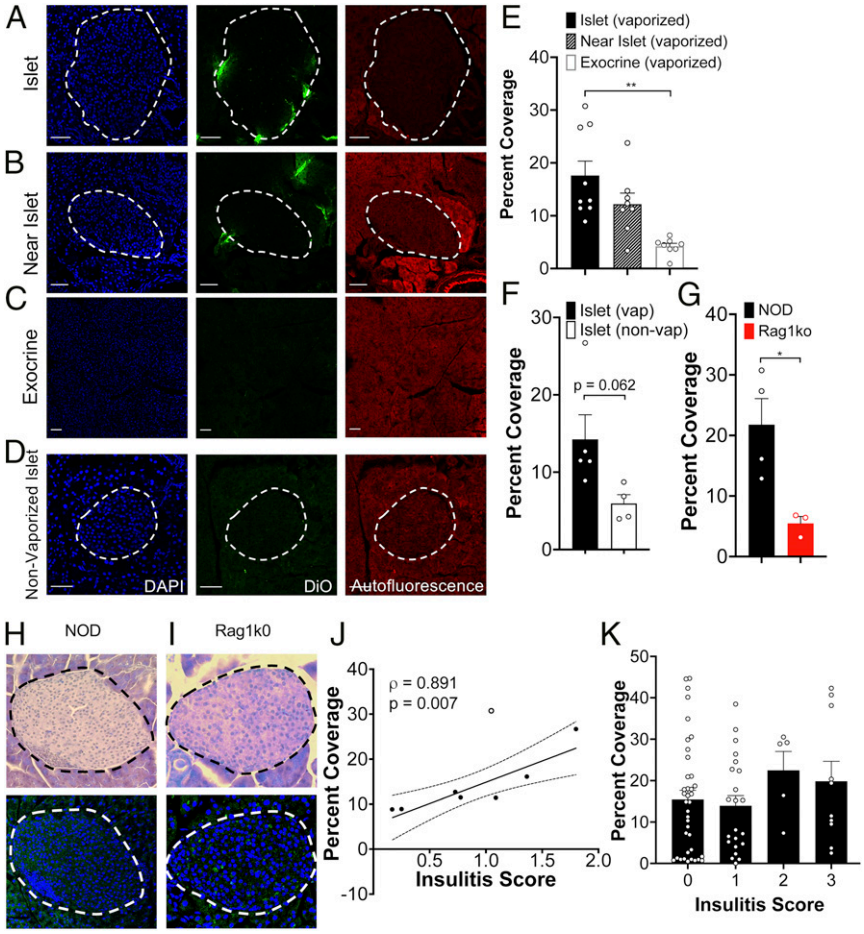

Fig. 4. Histological assessment of ND accumulation within the islets in T1D. (*A*) Representative confocal images of an islet within a pancreas section of 10-wk-old female NOD mouse following DiO-labeled ND infusion (green). Islet is circled with a dotted line, as determined from autofluorescence (red) and DAPI-labeling morphology (blue). (*B*) As in *A* for "near islet" (<200 μm from the islet) regions within the pancreas. (*C*) As in *A* for exocrine region far (>500 μm from the islet). (*D*) As in *A* but for female 10-wk-old NOD mice that did not receive ultrasound scans and therefore had no ND vaporization. (*E*) Mean DiO coverage in the islet, near islet regions, and exocrine tissue in 10-wk-old female NOD mice where NDs were vaporized. (*F*) Mean DiO coverage in the islet from 10-wk-old female NOD mice in which NDs were vaporized or nonvaporized. (*G*) Mean DiO coverage in the islet from 10-wk-old female NOD mice and 10-wk-old female Rag1ko mice. (*H*) Representative image of H&E-stained pancreas sections of 10-wk-old NOD mice, together with DiO fluorescence in neighboring tissue section. (*I*) As in *H* for pancreas sections of 10-wk-old NOD;Rag1ko mouse. (*J*) Scatterplot of the mean DiO fluorescent coverage of islets within the pancreas versus the mean insulitis score within the pancreas for NOD mice. (*K*) Mean DiO fluorescent coverage of islets within the pancreas that show insulitis scores of 0, 1, 2, or 3 (see *Materials and Methods*). Error bars in *E*, *F*, *G*, and *K* represent SEM. Trend line in *J* indicates linear regression with 95% CIs. Empty data point in indicates outlier. Outlier analysis used the Cook's distance: mean distance all points = 0.0808; outlier = 0.3803 (>3 times mean Cook's distance). Data in *E* represents $n = 8$ mice (142 islets and 27 exocrine regions). Data in *F* (Vaporized) represents $n = 5$ mice (89 islets) and (nonvaporized) represents $n = 4$ mice (37 islets). Data in *G* (NOD) represents $n = 4$ mice (53 islets) and (Rag1ko) represents $n = 3$ mice (31 islets). Data in *J* represents $n = 8$ NOD mice (112 islets). Data in *K* represents $n = 8$ NOD mice (75 islets). (Scale bar, 50 μm in *A* through *D*.) The *P* value in *E* is 0.0024 (**$P < 0.01$) and in *G* is 0.0255 (*$P < 0.05$), comparing groups indicated (unpaired Student's *t* test for data in *E*, *F*, and *G*; ANOVA for data in *K*). A mixed-effects model was used to assess the statistical significance and generate the regression in *J*.

localize to the islet regions of the pancreas dependent on the overall immune-infiltrated state of the pancreas.

Discussion

There are limited means for detecting insulitis and β-cell mass decline during the presymptomatic phase of T1D. A means to detect disease progression during this phase would guide therapeutic treatment during a window in which most β-cell mass remains, together with assessing the success of therapeutic intervention on disease progression prior to diabetes onset. The islet microvasculature increases permeability as a result of immune cell infiltration (insulitis). NDs are submicron-sized and thus can access permeable tissue (21), and following vaporization into microbubbles show a high scattering cross-section. Our goal was to test if submicron-sized NDs would specifically accumulate within immune-infiltrated islets during this presymptomatic phase and whether these NDs could be vaporized to provide elevated ultrasound contrast specifically in the pancreas (Fig. 5).

ND Accumulation in Presymptomatic T1D Correlates with Insulitis and Diabetes Progression. Our results demonstrated that NDs specifically accumulate within the pancreatic islets during the progression of insulitis in presymptomatic T1D. We observed significant contrast elevation within the pancreas following infusion and clearing from circulation, indicating that droplets had accumulated and vaporized within the pancreas. Notably, a contrast elevation was absent in noninfiltrated organs (e.g., kidney) within the NOD model of T1D (Fig. 1). Contrast elevation was also absent in the pancreas of immune-deficient Rag1ko mice that lack insulitis and do not develop diabetes (Fig. 2). Thus we conclude that NDs specifically accumulate within the organs in which immune infiltration and inflammation occur. Via histological analysis we further determined that within the pancreas accumulation was specific to

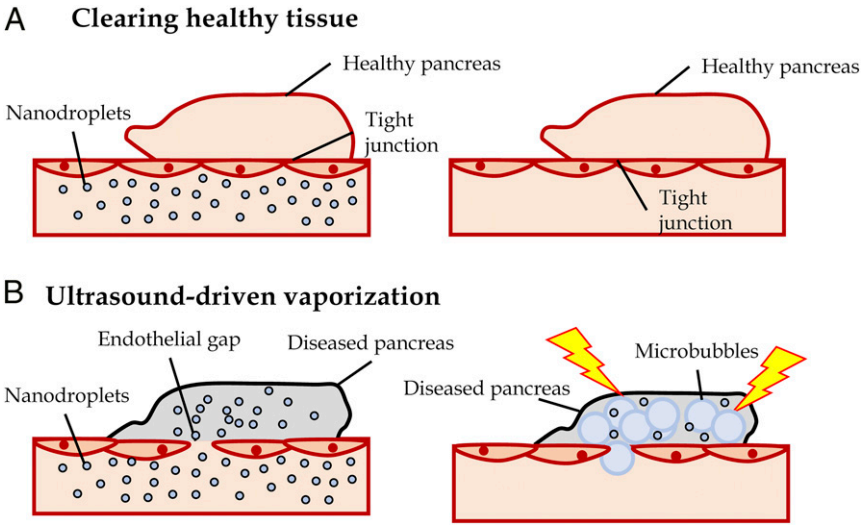

Fig. 5. Summary of experiments demonstrating NDs accumulate in immune-infiltrated islets and show increase contrast signal within the pancreas after vaporization. (*A*) After NDs are infused, the healthy islet microvasculature is not permeable (*Left*), and NDs are cleared from the blood stream (*Right*). (*B*) Immune-infiltrated islets in presymptomatic T1D have high vascular permeability and infused NDs accumulate in the tissue (*Left*). Following clearing from the vasculature, vaporization of accumulated NDs provides a source of increased subharmonic contrast (*Right*). This contrast signal therefore provides a measure of insulitis and thus presymptomatic T1D.

the regions (islets) that underwent immune infiltration. The correlation between ND accumulation within islet regions with the level of insulitis across the pancreas further supports the specificity of ND accumulation.

While we observed a strong correlation between insulitis and ND accumulation on a pancreas-wide basis, we did not see any link between insulitis and accumulation on an islet-wide basis. That is within a pancreas that on average showed high levels of insulitis, islets with lower or even absent insulitis still showed significant ND accumulation (Fig. 4*K*). When examined, this has been observed with other contrast agents that extravasate and accumulate within the islet in models of T1D (13, 15, 24). Thus, while islet microvascular permeability is a good indication of presymptomatic T1D (13, 14), it does not necessarily reflect spatial variations in insulitis across the pancreas, at least in mouse models of T1D. Testing whether there is a link between spatial variations in insulitis and islet microvascular permeability in human T1D is still needed. Nevertheless, the specific mechanisms leading to increased islet permeability concurrent with insulitis is still unknown and will be needed to identify the mechanisms underlying T1D that are reflected by such contrast accumulation measurements, such as the method described here.

Thus ND accumulation and contrast elevation upon vaporization provides a noninvasive method to assess the state of insulitis across the pancreas in T1D, prior to T1D onset at a point where animals are euglycemic.

ND Accumulation Predicts Disease Effectively. A key goal for imaging diagnostics for T1D is to detect signatures of presymptomatic T1D early, where significant β-cell mass remains and thus therapeutic treatment can be most effective (2). Predicting T1D onset may also avoid complications associated with diabetic ketoacidosis (7). We detected elevated contrast prior to diabetes onset where animals were euglycemic, that was absent in immunodeficient mice that did not develop diabetes, or was lower at 4 to 7 wk of age when insulitis is lower. Importantly, the contrast signal we measured following ND vaporization correlated with the time to diabetes onset (Fig. 3*C*): those animals that showed high-contrast elevation proceeded to diabetes more rapidly. This indicates an ability to predict the progression to T1D, which will be important to determine the time for therapeutic intervention and to assess the success of this intervention. Of further importance, while the contrast elevation was lower at 4 to 7 wk of age, it was above baseline levels in the majority of animals (e.g. as measured in Rag1ko mice), suggesting an ability to detect even very low levels of insulitis early in presymptomatic T1D progression. At these time points, fewer cases of insulin autoantibodies were detected (Fig. 3 *E* and *F*), which was also consistent with prior studies (23).

Future work will need to test whether ND accumulation, vaporization, and contrast elevation can predict the success of therapeutic treatments. Furthermore, future work will need to determine whether c-peptide preservation and T1D prevention is more effective at the stages at which signatures of presymptomatic T1D are detected using the method described here, compared to, for example, the presence of dysglycemia or following T1D onset. Such rigorous analysis has not been performed using any contrast agent.

Thus ND accumulation and contrast elevation provides a method to predict the rapid onset of T1D, which may be useful for therapeutic treatment.

Relevance to Clinical Application. While we have demonstrated high utility for ND-based ultrasound measurements in mouse models of T1D, there are important considerations to be made for clinical translation to human presymptomatic T1D detection and tracking. Iron-oxide nanoparticle MRI contrast agents selectively accumulate within the pancreata of animal models of T1D as well as recent onset human T1D (14, 25). Thus, in human T1D, there is increased microvascular permeability at diabetes onset, although prior to onset the time-course of islet microvascular permeability is unknown. This compared to increased microvascular permeability in the NOD mouse as early as 4- to 6-wk-old mice (15). Furthermore, while the EPR effect occurs in human T1D, it will be important to know how permeability compares to insulitis in the human pancreas.

Microbubble contrast agents are clinically approved, including within pediatric subjects (26). While use for pancreas indications is not approved, several off-label studies have been reported for pancreatic cancer and pancreatitis (27, 28). Thus, imaging ultrasound contrast in the pancreas in human subjects is feasible. While we utilized a small animal ultrasound machine in this study, NDs can be vaporized using clinical ultrasound frequencies (29, 30). Higher frequencies may be more suitable for pediatric subjects,

and the pancreas can be imaged using higher frequencies via endoscopic ultrasound (28).

While microbubble formulations such as DEFINITY are clinically approved, NDs have not been to date. However, NDs can be readily generated from microbubble contrast agents with minimal intervention (19): here, we condensed microbubbles using low temperature and high pressure only. Furthermore, we demonstrated NDs generated from a DEFINITY-like polydisperse formulation of microbubbles accumulated specifically within the islets of the pancreas and generated ultrasound contrast upon vaporization (Fig. 4 and *SI Appendix*, Fig. S3). Nanodroplets have also been generated from DEFINITY itself (20). Importantly, we injected comparable numbers of NDs as prior studies that utilized microbubbles, pointing to the efficiency of ND usage.

As such, while changes within the islet microvasculature during presymptomatic T1D still requires characterization, there is feasibility to translate the methods here to human T1D.

Summary. In summary, we demonstrate that ND ultrasound contrast agents specifically accumulate within the islets of animal models of T1D, where this accumulation can be measured via contrast-enhanced ultrasound following ND vaporization. This accumulation can inform both on the level of insulitis across the pancreas and the rapid progression to T1D. This method may be translatable to human presymptomatic T1D to guide therapeutic intervention to prevent T1D.

Materials and Methods

Animals. All animal procedures were performed in accordance with protocols (#00024) approved by the Institutional Animal Care and Use Committee of the University of Colorado Anschutz Medical campus. Female NOD mice were purchased from Jackson Laboratories at age 8 wk and imaged at 10 wk of age. Female Rag1ko animals were bred in-house and imaged at 10 wk of age. Throughout the study, animals were monitored weekly for blood glucose concentration utilizing a blood glucometer (Bayer).

ND Synthesis. Microbubbles were formed using previously published methods (31). Briefly DPPC and DSPE-PEG2000 (5:1 weight ratio) were dissolved in chloroform and evaporated into a lipid film. This film was reconstituted into PBS, and the mixture was sonicated with an ultrasonic probe at low power while bubbled with perfluorobutane, to generate a suspension of gas-filled microbubbles. The solution was then placed in an ice bath until the solution temperature was 23 °C; 4- to 5-μm-size isolated bubbles were then formed via a series of differential centrifugation steps and PBS washing. Size distributions and concentrations of the microbubbles were measured by laser light scattering and obscuration using the Accusizer 780A.

Condensation of microbubbles into NDs (19, 32) was achieved by cooling a suspension of microbubbles in PBS down to ∼1 °C in an isoflurane bath. A high pressure (∼10 bar) of perfluorobutane was then applied until the solution turned transparent. Size distributions and concentrations of the NDs were measured using the Accusizer 780A.

Polydisperse NDs were formed initially by reconstituting a DPPC:DSPE-PEG2000 film in PBS as above. This solution was then mechanically agitated using a Vialmix. Fluorescent labeling of NDs by DiO was achieved by diluting the lipid film mixture with 6 μM DiO.

Contrast-Enhanced Ultrasound Imaging. General anesthesia was established with isoflurane inhalation for ∼40 to 50 min for all mice imaged. A custom made 27G 1/2″ winged infusion set (Terumo BCT) was attached to a section of polyethylene tubing (0.61 OD × 0.28 ID, Warner Instruments) and inserted into a lateral tail vein. Abdominal fur was removed using depilatory cream, and ultrasound gel was placed to match the acoustic impedance between the mouse and transducer. Electrocardiogram, respiration rate, and body temperature were monitored by foot pad electrodes on the ultrasound platform. Body temperature and respiration rate were monitored throughout the imaging session.

A VEVO 2100 small animal high-frequency ultrasound machine (Visual Sonics, Fujifilm) was used for the experiments. A MS250 linear array transducer at 18 MHz was used. Conventional B-mode imaging was performed prior to ND infusion to identify the pancreas body in relation to the stomach, kidney, and spleen (Fig. 1*B*). Following successful identification, a region of interest was defined either around the pancreas (also encompassing the spleen) or around the kidney, and subharmonic contrast mode was initiated to specifically detect bubble-derived signal. Acquisition settings were set to transmit power, 10% (MI = 0.12); frequency, 18 MHz; standard beam width; contrast gain, 30 dB; 2D gain, 18 dB; and acquisition rate, 26 frames/s. Gating to remove breathing movement was carried out manually or using custom MATLAB scripts (Mathworks).

Background images were acquired for 3 min, at 30-s intervals, prior to ND infusion. NDs were then infused as a single bolus of 100 μL solution 2×10^8 ND/mL into the lateral tail vein. Following a 25-min pause, images were acquired for 10 min at 30-s intervals.

The vaporized ND contrast signal was background subtracted by the mean contrast intensity taken prior to ND infusion. Each time course was normalized to the preinfusion background values to provide the S-B/B. B-mode imaging was used to identify the pancreas and kidney and regions of interest were placed on the organs. The regions of interest were manually adjusted prior to analysis to avoid small regions of high-contrast saturation in the background images.

Histology and Insulitis Morphology. For assessment of insulitis, animals were anesthetized by intraperitoneal injection of ketamine (80 mg/kg) and xylazine (16 mg/kg) until no longer reactive to toe pinch. The pancreata were isolated, and mice were euthanized by exsanguination and/or bilateral thoracotomy. Pancreata were fixed in paraformaldehyde at 4 °C in a mechanical rocker overnight and embedded in optimal cutting temperature (OCT) blocks the following day; 8 μm sections were taken at three tissue depths. Alternating slices were stained with H&E for evaluation of islet T-cell infiltration. Images were acquired on an Eclipse-Ti wide-field microscope with a 20× 0.75 NA Plan Apo objective with a color charge-coupled device camera.

Images of islets were scored based on the extent of infiltration/insulitis: grade 0, no insulitis; grade 1, peri-insulitis with immune infiltrate bordering; grade 2, immune infiltrate penetrating the islet, covering <50% of the islet area; and grade 3, immune infiltrate penetrating the islet, covering >50% of the islet area. A minimum of three different tissue depths and at least 30 nonoverlapping islets per animal were analyzed. Weighted averages were calculated for each animal.

For assessment of ND coverage, 10-wk-old female NOD mice (JAX) received a single bolus injection of 100 μL solution of 2×10^8 ND/mL of DiO-labeled NDs. Following contrast imaging, mice were anesthetized by intraperitoneal injection of ketamine (80 mg/kg) and xylazine (16 mg/kg). The pancreas was dissected and fixed in 4% PFA on ice for 1 h and cryoprotected in 30% sucrose overnight or until the tissue sank. Pancreata were embedded in OCT medium, frozen in cryomolds, and cryo-sectioned at 8 μm sections, as above. Sections were imaged on an LSM800 confocal microscope (Zeiss), with at 488 nm excitation using a 20× 0.8 NA objective and pinhole settings to provide 1 μm z-section thickness throughout the tissue depth. Separate images were taken of exocrine tissue at locations anatomically isolated (>500 μm) from the islets. Islet regions were defined by autofluorescence and DAPI labeling. Near-islet regions were defined as within 200 μm of the islet. DiO coverage was calculated in MATLAB as the area of DiO positive pixels (pixels with fluorescence intensity significantly above the background fluorescence intensity) across the islet, or other defined region, and expressed as a fraction of total area imaged of the defined region.

Data Availability. All data and analysis are available to be shared upon request. Raw data, including czi microscopy files (for histology), Vevo ultrasound data files (for ultrasound images), and glucose and mIAA data have been deposited at https://www.ebi.ac.uk/biostudies/studies/S-BIAD189.

ACKNOWLEDGMENTS. R.K.P.B. (University of Colorado) is the guarantor of this work and, as such, had full access to all the data in the study and takes responsibility for the integrity of the data and the accuracy of the data analysis. This work was supported by Juvenile Diabetes Research Foundation Grants 1-INO-2017-435-A-N and 5-CDA-2014-198-A-N, as well as NIH Grants R01 DK102950 and R01 DK106412 (to R.K.P.B.), F31 DK121488 (to D.G.R.), TL1 TR002533 (to M.C.), and R01CA195051 (to M.A.B.). The funders had no role in the study design, data collection and analysis, decisions to publish, or preparation of the manuscript.

1. G. S. Eisenbarth, Type I diabetes mellitus. A chronic autoimmune disease. *N. Engl. J. Med.* **314**, 1360–1368 (1986).
2. R. A. Insel *et al.*, Staging presymptomatic type 1 diabetes: A scientific statement of JDRF, the Endocrine Society, and the American Diabetes Association. *Diabetes Care* **38**, 1964–1974 (2015).
3. K. C. Herold *et al.*, Anti-CD3 monoclonal antibody in new-onset type 1 diabetes mellitus. *N. Engl. J. Med.* **346**, 1692–1698 (2002).
4. K. C. Herold, B. N. Bundy, J. P. Krischer; Type 1 Diabetes TrialNet Study Group, Teplizumab in relatives at risk for type 1 diabetes. Reply. *N. Engl. J. Med.* **381**, 1880–1881 (2019).

5. A. G. Ziegler *et al*., Seroconversion to multiple islet autoantibodies and risk of progression to diabetes in children. *JAMA* **309**, 2473–2479 (2013).
6. E. Bonifacio, Predicting type 1 diabetes using biomarkers. *Diabetes Care* **38**, 989–996 (2015).
7. A. G. Ziegler *et al*.; Fr1da Study Group, Yield of a public health screening of children for islet autoantibodies in Bavaria, Germany. *JAMA* **323**, 339–351 (2020).
8. T. Singhal *et al*., Pancreatic beta cell mass PET imaging and quantification with [11C] DTBZ and [18F]FP-(+)-DTBZ in rodent models of diabetes. *Mol. Imaging Biol.* **13**, 973–984 (2011).
9. P. Wang *et al*., GLP-1R-targeting magnetic nanoparticles for pancreatic islet imaging. *Diabetes* **63**, 1465–1474 (2014).
10. F. R. Roberts *et al*., Possible type 1 diabetes risk prediction: Using ultrasound imaging to assess pancreas inflammation in the inducible autoimmune diabetes BBDR model. *PLoS One* **12**, e0178641 (2017).
11. J. R. St Clair, D. Ramirez, S. Passman, R. K. P. Benninger, Contrast-enhanced ultrasound measurement of pancreatic blood flow dynamics predicts type 1 diabetes progression in preclinical models. *Nat. Commun.* **9**, 1742 (2018).
12. M. C. Denis, U. Mahmood, C. Benoist, D. Mathis, R. Weissleder, Imaging inflammation of the pancreatic islets in type 1 diabetes. *Proc. Natl. Acad. Sci. U.S.A.* **101**, 12634–12639 (2004).
13. S. E. Turvey *et al*., Noninvasive imaging of pancreatic inflammation and its reversal in type 1 diabetes. *J. Clin. Invest.* **115**, 2454–2461 (2005).
14. J. L. Gaglia *et al*., Noninvasive imaging of pancreatic islet inflammation in type 1A diabetes patients. *J. Clin. Invest.* **121**, 442–445 (2011).
15. D. G. Ramirez *et al*., Contrast-enhanced ultrasound with sub-micron sized contrast agents detects insulitis in mouse models of type1 diabetes. *Nat. Commun.* **11**, 2238 (2020).
16. H. Wu *et al*., Time-intensity-curve analysis and tumor extravasation of nanobubble ultrasound contrast agents. *Ultrasound Med. Biol.* **45**, 2502–2514 (2019).
17. O. D. Kripfgans, J. B. Fowlkes, D. L. Miller, O. P. Eldevik, P. L. Carson, Acoustic droplet vaporization for therapeutic and diagnostic applications. *Ultrasound Med. Biol.* **26**, 1177–1189 (2000).
18. P. A. Mountford, M. A. Borden, On the thermodynamics and kinetics of superheated fluorocarbon phase-change agents. *Adv. Colloid Interface Sci.* **237**, 15–27 (2016).
19. P. S. Sheeran, S. H. Luois, L. B. Mullin, T. O. Matsunaga, P. A. Dayton, Design of ultrasonically-activatable nanoparticles using low boiling point perfluorocarbons. *Biomaterials* **33**, 3262–3269 (2012).
20. S. A. Choudhury, F. Xie, P. A. Dayton, T. R. Porter, Acoustic behavior of a reactivated, commercially available ultrasound contrast agent. *J. Am. Soc. Echocardiogr.* **30**, 189–197 (2017).
21. R. J. Paproski *et al*., Porphyrin nanodroplets: Sub-micrometer ultrasound and photoacoustic contrast imaging agents. *Small* **12**, 371–380 (2016).
22. D. Ize-Ludlow *et al*., Progressive erosion of β-cell function precedes the onset of hyperglycemia in the NOD mouse model of type 1 diabetes. *Diabetes* **60**, 2086–2091 (2011).
23. L. Yu *et al*., Early expression of antiinsulin autoantibodies of humans and the NOD mouse: Evidence for early determination of subsequent diabetes. *Proc. Natl. Acad. Sci. U.S.A.* **97**, 1701–1706 (2000).
24. Z. Medarova *et al*., Noninvasive magnetic resonance imaging of microvascular changes in type 1 diabetes. *Diabetes* **56**, 2677–2682 (2007).
25. J. L. Gaglia *et al*., Noninvasive mapping of pancreatic inflammation in recent-onset type-1 diabetes patients. *Proc. Natl. Acad. Sci. U.S.A.* **112**, 2139–2144 (2015).
26. S. J. Back *et al*., Pediatric contrast-enhanced ultrasound in the United States: A survey by the Contrast-Enhanced Ultrasound Task Force of the Society for Pediatric Radiology. *Pediatr. Radiol.* **48**, 852–857 (2018).
27. T. Ripollés, M. J. Martínez, E. López, I. Castelló, F. Delgado, Contrast-enhanced ultrasound in the staging of acute pancreatitis. *Eur. Radiol.* **20**, 2518–2523 (2010).
28. C. F. Dietrich, B. Braden, M. Hocke, M. Ott, A. Ignee, Improved characterisation of solitary solid pancreatic tumours using contrast enhanced transabdominal ultrasound. *J. Cancer Res. Clin. Oncol.* **134**, 635–643 (2008).
29. A. N. Thomas *et al*., Contrast-enhanced sonography with biomimetic lung surfactant nanodrops. *Langmuir* **37**, 2386–2396 (2021).
30. P. S. Sheeran *et al*., Methods of generating submicrometer phase-shift perfluorocarbon droplets for applications in medical ultrasonography. *IEEE Trans. Ultrason. Ferroelectr. Freq. Control* **64**, 252–263 (2017).
31. J. A. Feshitan, C. C. Chen, J. J. Kwan, M. A. Borden, Microbubble size isolation by differential centrifugation. *J. Colloid Interface Sci.* **329**, 316–324 (2009).
32. P. A. Mountford, S. R. Sirsi, M. A. Borden, Condensation phase diagrams for lipid-coated perfluorobutane microbubbles. *Langmuir* **30**, 6209–6218 (2014).